J. Fluid Mech. (1981), *vol.* 104, *pp.* 349-367
Printed in Great Britain

Experiments in nearly homogeneous turbulent shear flow with a uniform mean temperature gradient. Part 2. The fine structure

By STAVROS TAVOULARIS† AND STANLEY CORRSIN
Department of Chemical Engineering, The Johns Hopkins University, Baltimore, MD 21218

(Received 22 February 1980 and in revised form 23 June 1980)

Previous measurements in nearly homogeneous sheared turbulence with a uniform mean temperature gradient are here supplemented with data on the fine structure of the velocity and temperature fluctuation fields. The statistics of signal derivatives and of band-passed signals show that neither field is locally isotropic in the spectral range covered, possibly because of the insufficiently large turbulent Reynolds and Péclet numbers. Observed skewnesses of both velocity and temperature derivatives are explained qualitatively with the use of a kind of 'mixing-length' model. The flatness factors of the derivatives and of band-passed, high-frequency signals indicate appreciable departures from normality, consistent with the spatially 'spotty' fine structure. The temperature flatnesses are a bit larger than those of the streamwise velocity. The homogeneous shear flow data are compatible with measurements in turbulent boundary layers at comparable R_λ and $P_{\lambda\theta}$.

1. Introduction

In an earlier paper (Tavoularis & Corrsin 1981, hereafter referred to as I), it was reported that a nearly homogeneous turbulent shear flow with a nearly uniform mean temperature gradient is feasible. The flow field was basically the same as that of Harris, Graham & Corrsin (1977) with the superposition of a passive temperature field. Those two papers give details about the downstream evolution of the means and covariances of the velocity and temperature fields, and show that, away from the 'generator', the two fields develop asymptotically to an approximately self-similar region, retaining reasonable transverse homogeneity. Measurements included correlation functions, energy spectra, integral scales, microscales, and probability densities. The purpose of the experiment is, of course, to study turbulent transport in the absence of boundary effects or less drastic inhomogeneities.

In I, it was shown that heat transport characteristics are much like those of momentum transport, with the turbulent Prandtl number approximately 1·1, and that the temperature fluctuations are better correlated with the streamwise than the transverse velocity components. A main conclusion was that, as far as overall heat and momentum transport is concerned, this flow has some basic properties much like those of more general (inhomogeneous) turbulent shear flows. The present flow (and the one studied by Harris *et al.* 1977) has a Reynolds number $R_\lambda \approx 160$, larger than those of earlier

† Present address: Department of Mechanical Engineering, University of Ottawa, Ottawa, Canada K1N 6N5.

0022-1120/81/4692-3450 $02.00

realizations, and comparable to values commonly encountered in laboratory studies of inhomogeneous turbulence. This implies that considerable resemblance in the fine-scale structure with those inhomogeneous flows may exist. For example, the present flow appears suitable for the examination of the degree of local isotropy (Kolmogorov 1941) at this moderate R_λ. In particular, it is useful to know how well dissipation rates can be estimated from data on fewer than the full collection of terms, plus the assumption of isotropic dissipation. It would, of course, be desirable to increase R_λ much farther, but that was not feasible with the present apparatus.

An important small-scale property of high and moderate R_λ turbulence is the level of 'internal intermittency', i.e. spatial localization of the 'fine structure' – including dissipation. A quantitative measure is the flatness factor of the filtered turbulent velocity (Batchelor & Townsend 1949). Spatial intermittency in the streamwise direction is proportional to the temporal intermittency of a fixed-probe signal, through Taylor's 'frozen flow' approximation. Measurements of the flatness factor of the band-passed streamwise velocity were reported, for example, by Sandborn (1959) for a boundary layer, by Kennedy & Corrsin (1961) for a free shear layer, and by Kuo & Corrsin (1971) for a grid turbulence and an axisymmetric jet. Similar measurements for the internal intermittency of the temperature fluctuation apparently have not been published.

Signal derivatives emphasize information about the fine structures because differentiation of any Fourier component multiplies its amplitude by its wavenumber. Assuming that Kolmogorov's idea about the velocity field is valid, and assuming (Oboukhov 1949; Corrsin 1951) that it applies to the temperature field as well, local isotropy should exist for all fluctuations at sufficiently large wavenumbers, provided that the turbulence Reynolds and Péclet numbers are sufficiently large. For a proper test of local isotropy based on derivative statistics, the effects of large scales must be eliminated. Large-scale effects always increase the magnitude of even moments of the derivatives, but they can (at least in principle) have an either positive or negative contribution to the odd moments. The lowest-order, non-trivial, odd moment of the fluctuations is the third, in normalized form the skewness factor. With the exception of $S_{\partial u_i/\partial x_i}$ ($i = 1, 2, 3$, not summed), all skewnesses of the velocity and temperature derivatives should have zero contributions from locally isotropic wavenumber ranges. A non-zero value of such a skewness could indicate either that local isotropy is not applicable or that the large scales give a significant contribution to the derivative skewness.

Previous experiments include measurements of some velocity and temperature derivatives in a variety of turbulent flows. Emphasis has been recently placed on the (easily measurable) skewness of the streamwise temperature derivative, which was found to be non-zero in turbulent jets, wakes and boundary layers (for a summary, see Sreenivasan & Antonia 1978). Gibson, Friehe & McConnell (1977) identified a ramp-like large structure in the temperature signal in these flows and attributed it to the existence of a specific kind of large-scale 'coherent' structure. Sreenivasan & Antonia (1978) have shown that these large-scale ramps are responsible for most of the skewness. A systematic dependence of $S_{\partial\theta/\partial x_1}$ on the mean shear $\partial\overline{U}_1/\partial x_2$ and the mean temperature gradient $\partial\overline{T}/\partial x_2$ was demonstrated experimentally by Sreenivasan & Tavoularis (1980), who showed that in homogeneous turbulence $S_{\partial\theta/\partial x_1}$ is non-zero only when both $\partial\overline{U}_1/\partial x_2$ and $\partial\overline{T}/\partial x_2$ are non-zero; they also confirmed the relation (Gibson *et al.* 1977),

$$\operatorname{sgn}(S_{\partial\theta/\partial x_1}) = -\operatorname{sgn}\left(\frac{\partial\overline{U}_1}{\partial x_2}\right)\operatorname{sgn}\left(\frac{\partial\overline{T}}{\partial x_2}\right) \tag{1}$$

Although it is clear by now that the temperature-derivative skewness is mainly the result of large-scale anisotropy, it is not obvious how this anisotropy is produced and maintained. In some fields one can attribute it to large quasi-two-dimensional flow structures, which under certain conditions have been observed in some inhomogeneous flows, but this provides no explanation for the observed non-zero $S_{\partial\theta/\partial x_1}$ in homogeneous shear flow, where all available data have so far shown no such structures (see I). A homogeneous, qualitative explanation is attempted in the next section.

2. Derivative statistics

The experimental arrangement and the measuring techniques have been described in I and, in more detail, by Tavoularis (1978). Velocity fluctuations were measured with hot-wires (5·0 and 2·5 μm diameter) and temperature fluctuations with 'cold wires' (1·0 and 0·6 μm diameter) operating at a constant current of 0·25 mA. The streamwise derivatives were measured from temporal derivatives with the use of Taylor's 'frozen flow' approximation. The transverse derivatives of axial velocity were estimated by subtracting the signals of two parallel hot-wires, 1·25 mm long and 0·5 mm apart, and those of temperature by subtracting the signals of two 'cold wires' roughly 0·4 and 0·8 mm long and 0·6 mm apart minimum (the temperature-derivative data were obtained by extrapolating to zero wire separation the values corresponding to separations between 0·6 mm and 2 mm). All derivatives were corrected for electronic noise, while the temperature derivatives were corrected for velocity sensitivity of the 'cold wires', measured independently in the unheated flow. Corrections for the wire length and separation were computed following the analysis of Wyngaard (1968, 1969, 1971). The parallel probe data were not corrected for unequal frequency responses of the two wires (see Mestayer & Chambaud 1979); however, low-pass filtering of the two signals to identical cut-off frequencies (about 10 kHz for the velocity signals and 3 kHz for the temperature signals) was expected to reduce this error.

Table 1 contains the measured mean-squared derivatives as well as the corresponding locally isotropic estimates (computed from 'dissipation' rates estimated as the imbalance of transport and production via equations (2) and (6) of I). These results will be discussed in the next section.

Some interesting aspects of homogeneous shear flow are revealed by the skewness and flatness factors of various velocity and temperature derivatives,† also shown in table 1. A negative skewness of $\partial u_1/\partial x_1$ is a ubiquitous feature of turbulence, perceived as an effect of nonlinear interactions. Here $S_{\partial u_1/\partial x_1} \approx -0{\cdot}42$, a value consistent with measurements in other turbulent flows with comparable R_λ (see, for example, Tavoularis, Bennett & Corrsin 1978). The skewnesses of $\partial u_1/\partial x_3$, $\partial u_3/\partial x_1$, and $\partial\theta/\partial x_3$ are nearly zero, as expected because of symmetry with respect to x_3. The skewness of $\partial u_2/\partial x_1$ also appears to be nearly zero; however this value should be treated with caution, in view of the analysis by Gibson *et al.* (1977), showing that $S_{\partial u_2/\partial x_1}$ is liable to large experimental errors.

† Of all derivative data, the least accurate are probably the ones measured with the parallel-wire probes, which are subject to spatial resolution limitations, ambiguous determination of the exact distance between the wires, and errors caused by unequal time constants of the two wires. Such errors may be present in the mean-squared values; however, independent tests of the parallel-wire probes in grid-generated turbulence gave nearly zero transverse-velocity and temperature-derivative skewnesses, supporting the present finding that the observed skewnesses in shear flow describe (at least qualitatively) the physical process and are not an instrumentation artefact.

Quantity	Units	Mean-squared values: Measured	Corrected for wire length and separation	Locally isotropic estimates§	Percent difference	Skewness factor: Homogeneous shear flow	Skewness factor: Turbulent boundary layer	Flatness factor: Homogeneous shear flow	Flatness factor: Turbulent boundary layer
$\partial u_1/\partial x_1$	s^{-2}	11600	14100	15200	−7%	−0·42	−0·50†	6·5	7·0†
$\partial u_1/\partial x_2$	s^{-2}	46900	62500	30400	105%	0·62	—	7·3	—
$\partial u_1/\partial x_3$	s^{-2}	46200	61600	30400	103%	0·05	—	6·5	—
$\partial u_2/\partial x_1$	s^{-2}	14900	21300	30400	−30%	−0·05	—	7·0	—
$\partial u_3/\partial x_1$	s^{-2}	16400	23400	30400	−23%	0·00	—	7·0	—
$\partial\theta/\partial x_1$	$°C^2\ m^{-2}$	1100	1200	2800	−57%	−0·95	0·95‡	15·0	10·0‡
$\partial\theta/\partial x_2$	$°C^2\ m^{-2}$	1600	2200	2800	−21%	1·1	−1·2‡	11·0	6·5‡
$\partial\theta/\partial x_3$	$°C^2\ m^{-2}$	1600	2200	2800	−21%	0·0	0·0‡	10·0	7·0‡

† Ueda & Hinze (1975), $R_\lambda \approx 100$–150.

‡ Sreenivasan, Antonia & Danh (1977), $R_\lambda \approx 135$–175.

§ From 'dissipation' rates of the turbulent kinetic energy and the thermal fluctuations computed as the imbalance of transport and production by the mean gradients (I, equations (2) and (6)).

TABLE 1. Statistics of the velocity and temperature derivatives.

The most intriguing results are the appreciable skewnesses of $\partial u_1/\partial x_2$, $\partial\theta/\partial x_1$, and $\partial\theta/\partial x_2$, which depart sharply from their locally isotropic estimates of zero. A brief review of the literature did not reveal any previous measurements of $S_{\partial u_1/\partial x_2}$; the values of $S_{\partial\theta/\partial x_1}$ and $S_{\partial\theta/\partial x_2}$ were in close agreement with the boundary-layer values of Sreenivasan, Antonia & Danh (1977). The three skewnesses may be connected with the same local flow mechanism, in which case any qualitative explanation should cover them all. To summarize the existing information, in the absence of mean shear, $S_{\partial u_1/\partial x_2}$ should vanish by symmetry, while $S_{\partial\theta/\partial x_1}$ is experimentally negligible (Sreenivasan & Tavoularis 1980). $S_{\partial\theta/\partial x_1}$ changes sign whenever $\partial\overline{T}/\partial x_2$ does, and $S_{\partial\theta/\partial x_1} \approx 0$ whenever $\partial\overline{T}/\partial x_2 \approx 0$. The present data confirm equation (1); they also suggest the additional relations

$$\operatorname{sgn}(S_{\partial u_1/\partial x_2}) = \operatorname{sgn}\left(\frac{\partial\overline{U}_1}{\partial x_2}\right) \tag{2}$$

and

$$\operatorname{sgn}(S_{\partial\theta/\partial x_2}) = \operatorname{sgn}\left(\frac{\partial\overline{U}_1}{\partial x_2}\right)\operatorname{sgn}\left(\frac{\partial\overline{T}}{\partial x_2}\right). \tag{3}$$

Relation (3) is compatible with the boundary-layer data of Sreenivasan *et al.* (1977).

A unified qualitative explanation of the above observations is possible with the following model, inspired by the 'mixing-length' theories (e.g. Taylor 1915; Prandtl 1925; Nevzgljadov 1945). Consider a homogeneous shear flow with uniform, positive $\partial\overline{U}_1/\partial x_2$ and $\partial\overline{T}/\partial x_2$, as in figure 1. A lump of fluid starting at $x_2 = 0$ (where for convenience $\overline{U}_1 = 0$) performs a chance lateral motion to positions with either positive or negative x_2. If found at positive x_2, its streamwise velocity is lower than the local mean, so the fluid in the lump has $u_1 < 0$. Therefore a local stagnation region must develop on the upstream face of the 'alien' lump. This stagnation region is likely to have positive strain rates in the x_1, x_2 plane, so a fairly sharp 'internal interface' develops where most of the u_1 drop occurs. On the other hand, due to the effect of gross shear, an initially spherical (for simplicity) lump will assume a 'tilted oval' shape (in x_1, x_2), so that this interface will be also tilted away from the x_2, x_3 plane. Profiles of u_1 in the x_1 and x_2 directions across the lump would present a sharp drop-off across the interface and, subsequently, a relatively gradual increase, so that u_1 retains its correct average value. Therefore, a ramp-like structure of u_1 is implied with $S_{\partial u_1/\partial x_1} < 0$ and $S_{\partial u_1/\partial x_2} > 0$. The same signs of both skewnesses are produced, if the fluid lump has migrated to slower flow, at negative x_2.

Similar explanations are possible for the temperature-derivative skewnesses. Taking $\partial\overline{U}_1/\partial x_2 > 0$ and $\partial\overline{T}/\partial x_2 > 0$, at positive x_2, the lump of fluid has lower temperature than its surroundings so a sharp drop-off of θ occurs at its upstream boundary. The interface is tilted by the shear. As a result, $S_{\partial\theta/\partial x_1} < 0$ and $S_{\partial\theta/\partial x_2} > 0$. When $\partial\overline{U}/\partial x_2 = 0$, there are equal numbers of sharp drop-offs and sharp rises of both $\partial\theta/\partial x_1$ and $\partial\theta/\partial x_2$ and, consequently, $S_{\partial\theta/\partial x_1} \approx 0$ and $S_{\partial\theta/\partial x_2} \approx 0$. When $\partial\overline{T}/\partial x_2 = 0$, there is no preference for increase or decrease of temperature across an internal interface, so again $S_{\partial\theta/\partial x_1} \approx 0$ and $S_{\partial\theta/\partial x_2} \approx 0$. Inverting the temperature profile ($\partial\overline{T}/\partial x_2 < 0$) simply results in changing of the signs of both skewnesses, consistently with equations (1) and (3).†

The presented model attempts only a *qualitative* explanation for the algebraic signs

† Note added in proof: Consistent with the present model, the skewnesses of all three temperature derivatives were found to be negligible in the same homogeneous shear flow but with dominant $\partial\overline{T}/\partial x_3$ (Tavoularis & Corrsin, manuscript in preparation).

of the skewnesses. The physical mechanism for the initiation of the lump migration is not touched upon. A more detailed experimental study should involve the simultaneous monitoring of the four derivatives, $\partial u_1/\partial x_1$, $\partial u_1/\partial x_2$, $\partial\theta/\partial x_1$, and $\partial\theta/\partial x_2$, and a statistical analysis of the length, orientation, amplitude, and relative frequency of occurrence of the large strain rate sheets. Such information is not yet available; however, preliminary direct measurements show that

$$\overline{\frac{\partial\theta}{\partial x_1}\frac{\partial\theta}{\partial x_2}}\Big/\left(\frac{\partial\theta}{\partial x_1}\right)'\left(\frac{\partial\theta}{\partial x_2}\right)' \approx -0{\cdot}48.$$

An independent estimate of this correlation coefficient from the $R_{\theta\theta}(r_1, r_2, 0; 0)$ iso-correlation contours (assuming that the family of similar ellipses of figure 14(*a*) in I includes cases with $r/\lambda \ll 1$) was $-0{\cdot}50$. A related correlation estimated from the $R_{11}(r_1, r_2, 0; 0)$ iso-correlation contours (figure 10, Harris *et al.* 1977) was

$$\overline{\frac{\partial u_1}{\partial x_1}\frac{\partial u_1}{\partial x_2}}\Big/\left(\frac{\partial u_1}{\partial x_1}\right)'\left(\frac{\partial u_1}{\partial x_2}\right)' \approx -0{\cdot}44.$$

The above results are compatible with the speculation that, with high probability, large excursions of the derivatives $(\partial u_1/\partial x_1, \partial u_1/\partial x_2)$ and $(\partial\theta/\partial x_1, \partial\theta/\partial x_2)$ occur simultaneously. Furthermore, the signs of the two derivative correlations are compatible with the qualitative model of figure 1.

Table 1 also contains the flatness factors of various velocity and temperature derivatives. All were substantially higher than 3·0 (the value for a normal random variable), consistent with an intermittent nature of the dissipation of the turbulent energy and the thermal 'energy'. All velocity derivative flatnesses were roughly equal to 7, which is also the value of $F_{\partial u_1/\partial x_1}$ in a turbulent boundary layer with comparable R_λ (Ueda & Hinze 1975).

In contrast, $F_{\partial\theta/\partial x_1}$ is about 50 % larger than $F_{\partial\theta/\partial x_2}$ and $F_{\partial\theta/\partial x_3}$, a difference which is too large to be attributed solely to measurement inaccuracies. This difference is a bit surprising because the increments of the F's above 3·0 are presumably a measure of intermittency (Bachelor & Townsend 1949), and it can be shown that, in a (hypothetical) homogeneous, binary (hence intermittent) scalar field, the intermittency is independent of direction. For a simple proof consider a two-dimensional, homogeneous binary scalar field (the extension to a three-dimensional scalar field is straightforward). The plane of the field can be completely covered with an infinite number of infinitesimally thin parallel strips, oriented in any direction. By homogeneity, the 'line intermittency' (i.e. the relative length of one phase) in each direction is independent of strip translation; thus it is equal to the 'area intermittency' (since, within each 'thin' strip, the 'line intermittency' is obviously equal to the 'area intermittency') of the whole plane and, therefore, it is independent of direction. Possibly the inequality of the F's of temperature gradient components is attributable in part to the fact that the $\partial\theta/\partial x_i$ field is not sharply bimodal. In any case, the relative values agree well with boundary-layer data at comparable turbulent Reynolds and Péclet numbers (Sreenivasan *et al.* 1977).

The available measurements of $F_{\partial\theta/\partial x_1}$ in air (figure 2) show that it increases monotonically with R_λ. Similar behaviour has been observed for $F_{\partial u_1/\partial x_1}$ (see for instance Kuo & Corrsin 1971). For a fixed R_λ, $F_{\partial\theta/\partial x_1}$ is appreciably larger than $F_{\partial u_1/\partial x_1}$, and this trend increases with increasing R_λ.

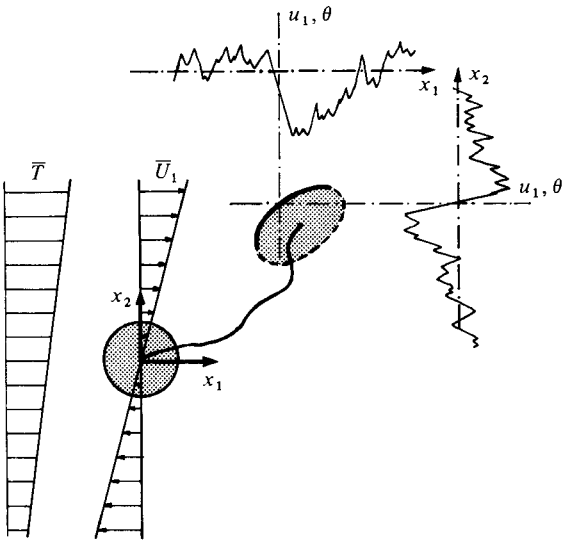

FIGURE 1. Qualitative explanation of the observed non-zero skewnesses in homogeneous sheared turbulence.

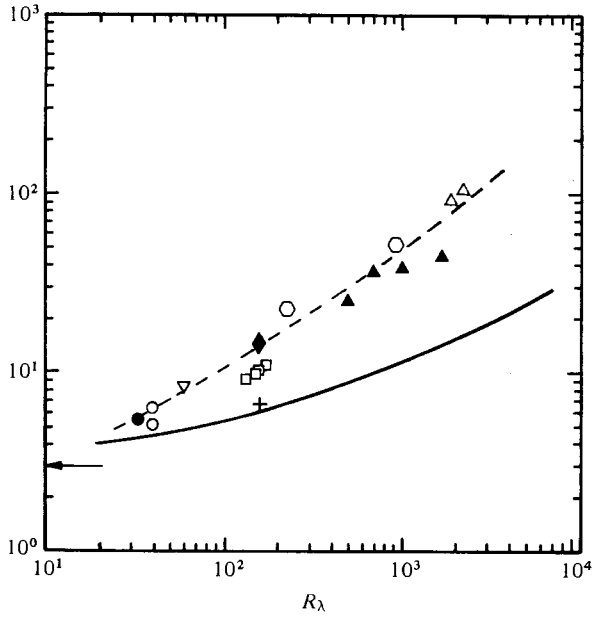

FIGURE 2. Flatness factors of the velocity and temperature derivatives in air flows. $F_{\partial u_1/\partial x_1}$: +, present data; ——, earlier data (from Kuo & Corrsin 1971). $F_{\partial\theta/\partial x_1}$: ◆, present data; ● grid turbulence (Sreenivasan *et al.* 1980); ○, grid turbulence (Antonia *et al.* 1978); □, boundary layer (Sreenivasan *et al.* 1977); ▽, pipe flow (Elena, Chauve & Dumas 1977); ▲, atmosphere (Gibson, Stegen & Williams 1970); △, atmosphere (Friehe *et al.* 1975); ⬡, jet (Gibson *et al.* 1977); – – –, faired curve.

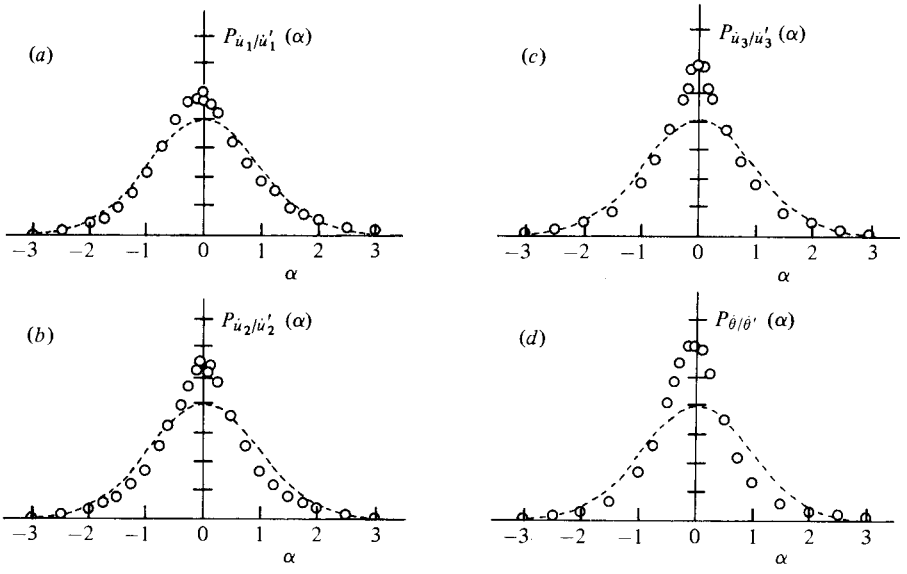

FIGURE 3. Probability density functions of the temporal derivatives of the turbulent velocities and temperature. ○, experimental values, – – –, normal distribution; overdots indicate temporal derivatives.

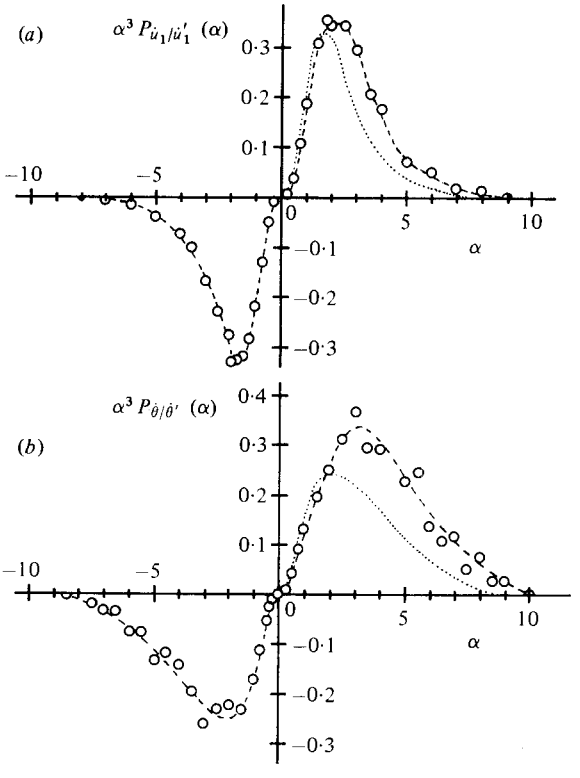

FIGURE 4. Computation of skewnesses as the third moments of the corresponding probability density functions. ○, experimental values; – – –, faired curves through the data; . . ., anti-symmetric curves; overdots indicate temporal derivatives.

The temporal (or, through Taylor's approximation, spatial streamwise) derivative probability density functions of the turbulent velocities and the temperature are shown in figure 3. All depart appreciably from normality, with peaks at the origin, consistent with their high flatness factors. Their degrees of asymmetry are qualitatively consistent with the directly measured skewnesses. As a check, the third moments of the probability densities of $\partial u_1/\partial t$ and $\partial\theta/\partial t$ are plotted (figure 4). The areas under the two curves are 0·60 and 1·15, relatively close to the directly measured skewnesses, 0·42 and 0·95.

3. The departure from local isotropy

Table 1 shows the percent difference between the measured values of several moments of the velocity and temperature derivatives and the corresponding locally isotropic estimates, computed from dissipation rates (see I). The 100 % differences in the variances of some velocity derivatives cannot be attributed solely to measurement inaccuracies. The ordering of variances was roughly as follows:

$$2\overline{\left(\frac{\partial u_1}{\partial x_1}\right)^2}\Big/\overline{\left(\frac{\partial u_1}{\partial x_2}\right)^2} \approx 2\overline{\left(\frac{\partial u_1}{\partial x_1}\right)^2}\Big/\overline{\left(\frac{\partial u_1}{\partial x_3}\right)^2} \approx 0{\cdot}45 \tag{4}$$

and

$$2\overline{\left(\frac{\partial u_1}{\partial x_1}\right)^2}\Big/\overline{\left(\frac{\partial u_2}{\partial x_1}\right)^2} \approx 2\overline{\left(\frac{\partial u_1}{\partial x_1}\right)^2}\Big/\overline{\left(\frac{\partial u_3}{\partial x_1}\right)^2} \approx 1{\cdot}3. \tag{5}$$

Both ratios are 1·0 in isotropic turbulence. Relations (5) are comparable to measurements in other moderate R_λ shear flows (Champagne 1978), but no previous measurements of the ratios (4) are known. Independent estimates from the iso-correlation contours show even larger departure from local isotropy:

$$2\overline{\left(\frac{\partial u_1}{\partial x_1}\right)^2}\Big/\overline{\left(\frac{\partial u_1}{\partial x_2}\right)^2} \approx 0{\cdot}40, \quad 2\overline{\left(\frac{\partial u_1}{\partial x_1}\right)^2}\Big/\overline{\left(\frac{\partial u_1}{\partial x_3}\right)^2} \approx 0{\cdot}28. \tag{4a}$$

Departures from local isotropy also are indicated by the temperature derivative variances. The direct measurements were

$$\overline{\left(\frac{\partial\theta}{\partial x_1}\right)^2}\Big/\overline{\left(\frac{\partial\theta}{\partial x_2}\right)^2} \approx \overline{\left(\frac{\partial\theta}{\partial x_1}\right)^2}\Big/\overline{\left(\frac{\partial\theta}{\partial x_3}\right)^2} \approx 0{\cdot}55, \tag{6}$$

in contrast to the isotropic value of 1·0. The two transverse temperature-derivative variances were, of course, measured by a procedure different from that used for $\overline{(\partial\theta/\partial x_1)^2}$, but again such differences can only in part be caused by measuring errors, mainly the uncertainty of corrections for the wire length and separation and the residual difference in the frequency responses of the two 'cold' wires. It is difficult to estimate the magnitude or the direction of such errors. However, the values computed from iso-correlation contours, namely

$$\overline{\left(\frac{\partial\theta}{\partial x_1}\right)^2}\Big/\overline{\left(\frac{\partial\theta}{\partial x_2}\right)^2} \approx 0{\cdot}45, \quad \overline{\left(\frac{\partial\theta}{\partial x_1}\right)^2}\Big/\overline{\left(\frac{\partial\theta}{\partial x_3}\right)^2} \approx 0{\cdot}35, \tag{6a}$$

agreed qualitatively with (6). In general, there is a qualitative resemblance between (4) and (6) and between (4*a*) and (6*a*).

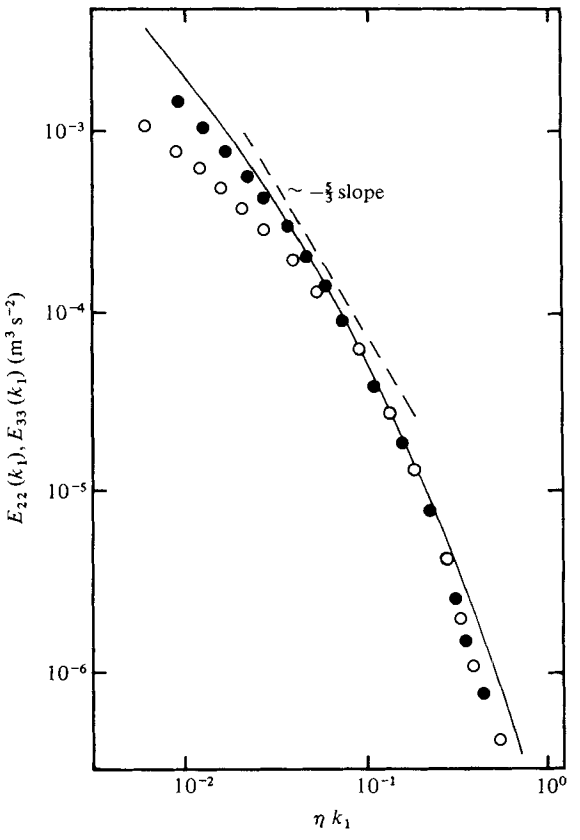

FIGURE 5. Spectral test of local isotropy. ○, $E_{22}(k_1)$; ●, $E_{33}(k_1)$, ——, $E_{22}^*(k_1)$, $E_{33}^*(k_1)$ (computed from $E_{11}(k_1)$).

The directly measured total 'thermal energy' (i.e. $\overline{\theta^2}$) destruction rate was about 30 % lower than the imbalance between production and convection of $\overline{\theta^2}$, emphasizing inaccuracies in the measuring techniques, and to some extent in the idealized analytical approximation of the problem (see I for more details).

Tests of the degree of local isotropy are possible through spectral analysis. One condition necessary for the expectation of a locally isotropic inertial range (hence dissipative range as well) in the turbulent energy spectrum is the existence of a range of wavenumbers k, satisfying the relations (Corrsin 1958)

$$\eta \left(\frac{d\overline{U}_1}{dx_2}\right)^{\frac{3}{2}} \Big/ (8\epsilon)^{\frac{1}{2}} \ll \eta k \ll 1. \tag{7}$$

In the present flow (at $x_1/h = 11{\cdot}0$) this becomes

$$0{\cdot}01 \ll \eta k \ll 1, \tag{7a}$$

which can be only marginally satisfied, if at all. A less restrictive condition was given by Bradshaw (1967) as

$$0{\cdot}03 \approx \frac{10\eta}{L} < \eta k < 0{\cdot}1. \tag{7b}$$

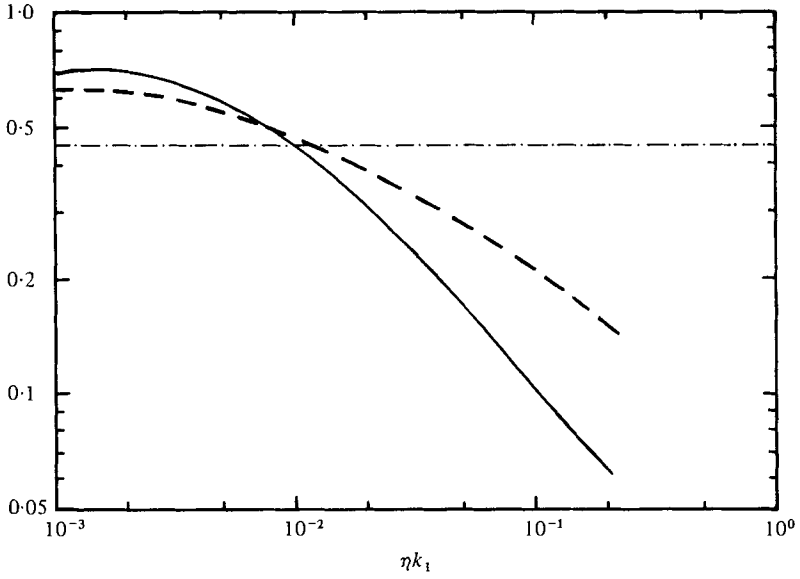

FIGURE 6. Coherencies of the shear-stress and of the transverse heat transport. ——, $|E_{12}|/(E_{11}E_{22})^{\frac{1}{2}}$; – – –, $|E_{\theta u_2}|/(E_{\theta\theta}E_{22})^{\frac{1}{2}}$; –·–, total shear-stress and heat transport correlation coefficients.

A necessary condition for local isotropy in the mixed inertial–viscous range (Corrsin 1958) is

$$(\epsilon/\nu)^{\frac{1}{2}} \gg d\overline{U}_1/dx_2. \tag{8}$$

Here $(\epsilon/\nu)^{\frac{1}{2}}/(d\overline{U}_1/dx_2) \approx 10$, so that this condition also is not well satisfied. Analogous conditions can be devised for the thermal fluctuation field.

A direct spectral test of local isotropy is given in figure 5, showing the measured one-dimensional spectra $E_{22}(k_1)$ and $E_{33}(k_1)$ as well as their estimate computed from the measured $E_{11}(k_1)$ with the use of the isotropic relation

$$E^*_{22}(k_1) = E^*_{33}(k_1) = \frac{1}{2}\left[E^*_{11}(k_1) - k_1\frac{\partial E^*_{11}(k_1)}{\partial k_1}\right]. \tag{9}$$

All spectra were corrected for errors due to the wire length and the cross-wire separation (Wyngaard 1968). It can be seen that

$$E^*_{22}(k_1) \approx E_{22}(k_1), \quad 0{\cdot}07 \leqslant \eta k_1 \leqslant 0{\cdot}02,$$

and

$$E^*_{33}(k_1) \approx E_{33}(k_1), \quad 0{\cdot}04 \leqslant \eta k_1 \leqslant 0{\cdot}02.$$

As estimated, there appears to be at most a negligible isotropic inertial range, (7*a*) or (7*b*). A Kolmogorov-type power law,

$$E_{22}(k_1) \propto k_1^{-\frac{5}{3}} \tag{10}$$

can be fitted to the data in the narrow range $0{\cdot}07 \leqslant \eta k_1 \leqslant 0{\cdot}10$, which is of course insignificant.

The two measured transverse spectra, $E_{22}(k_1)$ and $E_{33}(k_1)$, are roughly the same for $\eta k_1 > 0{\cdot}07$. Paradoxically, these spectra are lower than their locally isotropic estimates for $nk_1 > 0{\cdot}1$. This difference may be due partially to experimental inaccuracies (for

instance, insufficient correction for the cross-wire separation at high frequencies and errors due to difference in the frequency responses of the two hot-wires); nonetheless, it is consistent with the independent measurements of the mean-squared velocity derivatives, equation (4), and with velocity spectra in other shear flows at comparable R_λ (Champagne 1978).

The tendency towards isotropy of the small scales is indicated by the decreasing value of the narrow-band-passed turbulent shear stress and heat transport coherences (correlation coefficients) as the pass-band wavenumber increases (figure 6). The present results are reliable only up to wavenumbers roughly equal to one-fifth of the inverse Kolmogorov microscale, but the trends are clear. Both coherences are likely to be zero at sufficiently high wavenumbers because of local isotropy (e.g. Corrsin 1949; Laufer 1951). Based on figure 6, one could speculate that the temperature fluctuations depart more from local isotropy than do the velocity fluctuations. It may be relevant that the temperature derivatives are more skew than the velocity derivatives. Of course such a connexion is mere speculation, since velocity is a vector while temperature is a scalar, so exact analogies are impossible.

4. Band-passed signal statistics

A quantitative measure of the observed 'internal intermittency' (spatially localized 'fine structure', including the energy dissipation) in high Reynolds number turbulence is the flatness factor of the filtered turbulent velocity (Batchelor & Townsend 1949). Spatial intermittency in the streamwise direction is proportional to the temporal intermittency of a fixed-probe signal through Taylor's 'frozen flow' approximation. Following the procedures of Kuo & Corrsin (1971), the flatness factors of the band-passed signals for different values of the centre frequency,

$$f_m = (f_H f_L)^{\frac{1}{2}}, \tag{11}$$

are plotted against the relative bandwidth,

$$\Delta f/f_m = (f_H - f_L)/f_m; \tag{12}$$

f_H and f_H are, respectively, the low and high cut-off frequencies (-3 dB points) of the band-pass filter. A non-recursive, digital band-pass filter (described in the appendix) was used for all final measurements but some measurements were repeated using an analog band-pass filter for a comparison of the two techniques.

Figure 7 shows the flatness factor F_{u_1} of the band-passed streamwise turbulent velocity at $x_1/h = 11{\cdot}0$. For a fixed f_m, F_{u_1} increases with increasing $\Delta f/f_m$ from a value near 3·0 (the normal value), up to a maximum near $\Delta f/f_m = 0{\cdot}7$; then it decreases again, presumably to roughly 3·0, at sufficiently large $\Delta f/f_m$, which gives the full velocity fluctuation. For a fixed $\Delta f/f_m$, F_{u_1} increases with increasing f_m. The peak of F_{u_1} for a fixed f_m seems to shift slightly to lower $\Delta f/f_m$ as f_m increases.

Figure 7 also shows that F_{u_1} measured with the analog filter was significantly larger than that measured with the digital filter, for $\Delta f/f_m < 0{\cdot}8$. Consequently, the peak of the flatness factor of the analog-filtered velocity appears to be near $\Delta f/f_m \approx 0{\cdot}3$ instead of its correct position at $\Delta f/f_m \approx 0{\cdot}7$. This error is due to the non-uniform phase-shift of analog, band-passed signals. It must have been contained in the data of Kuo & Corrsin (1971), who reported peaking of F_{u_1} near $\Delta f/f_m \approx 0{\cdot}3$ in nearly isotropic turbulence.

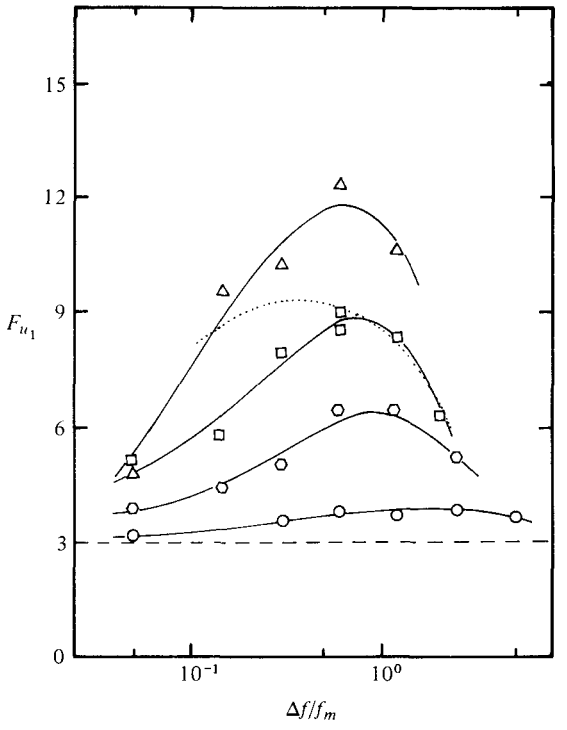

FIGURE 7. Flatness factor of the band-passed streamwise turbulent velocity. ○, $f_m/f_K = 0{\cdot}09$; ○, $f_m/f_K = 0{\cdot}27$; □, $f_m/f_K = 0{\cdot}45$; △, $f_m/f_K = 0{\cdot}64$ (digital filter); ..., $f_m/f_K = 0{\cdot}45$ (analog filter); Kolmogorov frequency, $f_K \equiv \bar{U}_1/(2\pi\eta) \approx 11$ kHz.

The internal intermittency of turbulent fine structure can be demonstrated also by the increase in the flatnesses of velocity derivatives (Batchelor & Townsend 1949). 'Compound' filtering, by differentiating the band-passed velocity, gives $F_{\partial u_1/\partial x_1}$ as plotted against $\Delta f/f_m$ in figure 8. Obviously, at sufficiently large $\Delta f/f_m$, $F_{\partial u_1/\partial x_1}$ should attain its full-band value, roughly 6·5. On the other hand, band-pass filtering with infinitely narrow bandwidth corresponds to 'infinite smoothing' (see Kuo & Corrsin 1971); for sufficiently small $\Delta f/f_m$, the effects of differentiation (counteracting smoothing) must be overcome, and $\partial u_1/\partial x_1$ must approach normality (although possibly for smaller $\Delta f/f_m$ than u_1 does). The measurements seem to be consistent with these requirements, at least for the cases with sufficient data. A curious effect is that the curves for $f_m = 1$ and 3 kHz increase monotonically with bandwidth, while that for $f_m = 5$ kHz increases at low $\Delta f/f_m$ to roughly 10 at $\Delta f/f_m \approx 1{\cdot}0$, then decreases again. The available data for $f_m = 7$ kHz are in qualitative agreement with the trends at smaller f_m.

It is plausible to expect that the temperature fluctuation will display 'internal intermittency' of the same character as that of the turbulent velocity, if the Reynolds and Péclet numbers are both large enough (Gibson & Masiello 1972). Indeed, all signals for the first-order temperature derivatives had a typically intermittent appearance (namely alternating regions of large- and small-amplitude fluctuations). Consistently, all corresponding flatnesses were significantly larger than 3·0. As that of the turbulent velocity, the internal intermittency of temperature fluctuations can

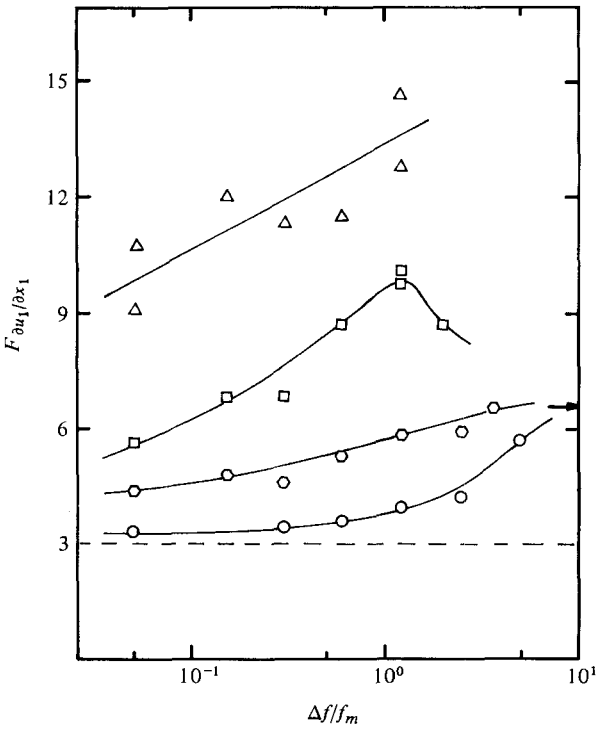

FIGURE 8. Flatness factor of the band-passed derivative of the streamwise turbulent velocity. Symbols as in figure 7.

be quantitatively represented by the departure of the flatness F_θ of the band-passed temperature from the normal value of 3·0.

Figure 9 shows F_θ as a function of $\Delta f/f_m$ for two values of f_m. The digital band-pass filter was also used and the data were corrected for electronic noise and for velocity sensitivity of the cold wire. F_θ shows the same behaviour as F_{u_1} although, quantitatively, the two families of curves are distinct. For a fixed f_m, F_θ has a maximum at $\Delta f/f_m$ between 1·0 and 2·0; it decreases monotonically on both sides of this maximum, and approaches 3·0 at high as well as low values of $\Delta f/f_m$. The position of the maximum is shifted to lower $\Delta f/f_m$ with increasing f_m. For the same f_m and $\Delta f/f_m$, F_θ is measurably larger than F_{u_1}; considering that band-pass filtering has an effect in part similar to that of differentiation, the above result is consistent with the fact the full-band $F_{\partial\theta/\partial x_1}$ is larger than the full-band $F_{\partial u_1/\partial x_1}$. It is displayed explicitly in figure 10.

This work was supported by the U.S. National Science Foundation, Program on Atmospheric Sciences. We thank Professor Frank Champagne for helpful suggestions, especially with respect to our parallel probes data.

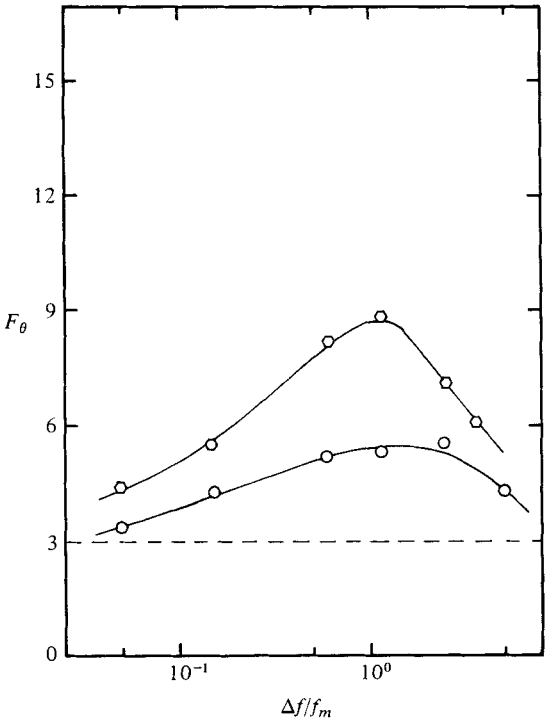

FIGURE 9. Flatness factor of the band-passed temperature. Symbols as in figure 7.

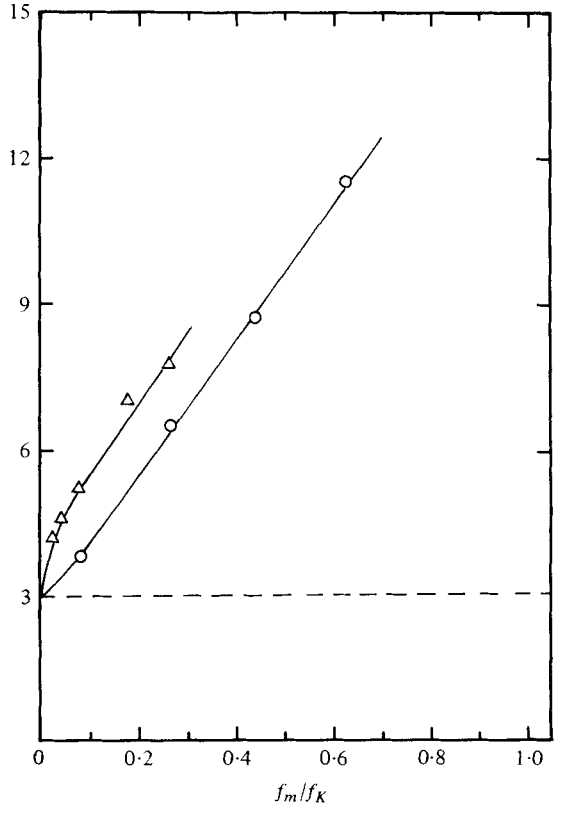

FIGURE 10. Flatness factors of the band-passed signals as functions of the mid-band frequency, for fixed relative bandwidth $\Delta f/f_m = 1{\cdot}0$. ○, F_{u_1}; △, F_θ.

Appendix. Digital band-pass filtering

Accurate measurement of higher (especially of odd-order) moments of filtered signals requires that the signal waveform within the prescribed pass-band be preserved. Consequently, filters introducing zero phase shift, or a phase shift proportional to frequency within their pass-band, are in order. Analog filters with such properties can be efficiently designed only for bandwidths much smaller than the centre frequency. With wider bandwidths, some analog filters may in fact introduce serious errors in the measurements of skewness and flatness factors of a filtered signal, although possibly preserving the band-passed mean-squared amplitude. For example, at bandwidth to centre frequency ratio equal to 1·5, the Krohn-Hite 330M (four-pole Butterworth) analog filter has a theoretical phase characteristic shown in figure 11. Measured with this filter, the skewness of the band-passed temperature streamwise derivative was (erroneously) found to change sign for bandwidth to centre frequency ratios roughly between 0·5 and 2·5.

A phase shift is a necessary consequence of the infinite interval impulse response of analog filters. In contrast, finite interval response digital filters with zero phase shift can be easily designed and implemented on a digital computer. The theory of digital filters can be found in textbooks of digital signal analysis, for example the one by Stearns (1975).

The output time history y_m of a non-recursive† digital filter with zero phase shift is computed from the input time history x_m as

$$y_m = b_0 x_m + \sum_{n=1}^{N} b_n (x_{m-n} + x_{m+n}), \tag{A 1}$$

where b_0, b_n are the cosine Fourier coefficients of the filter transfer function $H(\omega)$, namely

$$b_0 = \frac{\Delta t}{\pi} \int_0^{\pi/\Delta t} H(\omega)\, d\omega \tag{A 2}$$

and

$$b_n = \frac{\Delta t}{\pi} \int_0^{\pi/\Delta t} H(\omega) \cos(n\omega\, \Delta t)\, d\omega, \quad n = 1, 2, \ldots, N. \tag{A 3}$$

Any continuous $H(\omega)$ can therefore be approximated within any required accuracy by a finite Fourier series

$$\hat{H}(\omega) = b_0 + 2 \sum_{n=1}^{N} b_n \cos(n\omega\, \Delta t). \tag{A 4}$$

For an ideal band-pass filter with transfer function

$$H(\omega) = \begin{cases} 1, & \omega_L \leqslant \omega \leqslant \omega_H, \\ 0, & \text{otherwise}, \end{cases} \tag{A 5}$$

the coefficients b_0, b_n should be

$$b_0 = \frac{(\omega_H - \omega_L)\, \Delta t}{\pi} \tag{A 6}$$

and

$$b_n = \frac{\sin(n\omega_H\, \Delta t) - \sin(n\omega_L\, \Delta t)}{n\pi}, \quad n = 1, 2, \ldots, N. \tag{A 7}$$

† These are filters whose output does not explicitly depend on the past output values.

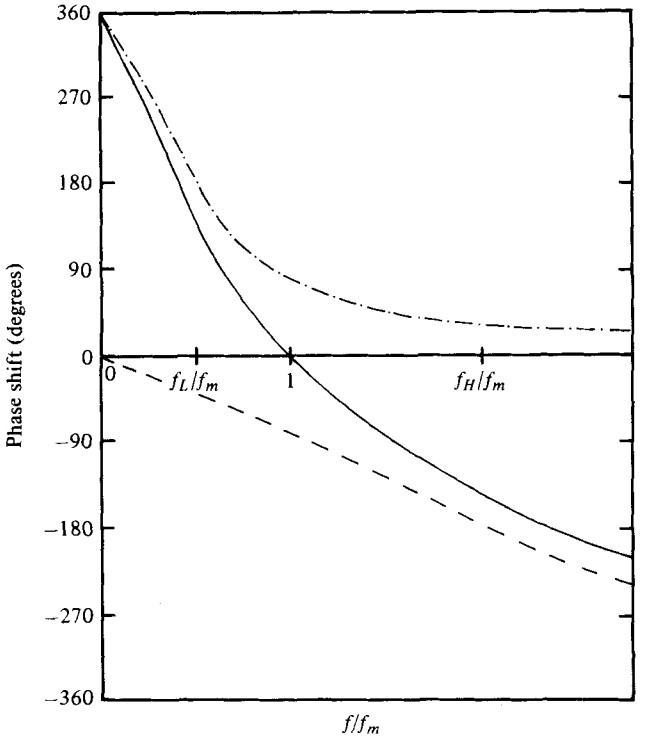

FIGURE 11. Theoretical phase characteristic of a four-pole Butterworth band-pass filter. —·—, high-pass section; – – –, low-pass section; ——, combined band-pass; $\Delta f/f_m = 1{\cdot}5$.

The truncation of the Fourier series (A 4) to a finite number of terms introduces the 'Gibbs phenomenon', namely an oscillatory form of the transfer function estimate. Smooth transfer functions can be obtained with the use of a 'window function' w_n, in which case expressions (A 1) and (A 4) are modified into

$$y_m = b_0 x_m + \sum_{n=1}^{N} b_n w_n (x_{m-n} + x_{m+n}) \tag{A 8}$$

and

$$\hat{H}(\omega) = b_0 + 2 \sum_{n=1}^{N} b_n w_n \cos(n\omega \Delta t). \tag{A 9}$$

The 'hanning window'

$$w_n = \frac{1}{2}\left(1 + \cos\frac{n\pi}{N}\right) \tag{A 10}$$

was used in the present study.

The transfer function estimate $\hat{H}(\omega)$ is periodic with period $\pi/\Delta t$. To avoid aliasing, the sampling time Δt should be less than π/ω_H and all frequencies above the high-frequency cut-off $f_H \equiv \omega_H/2\pi$ should be removed with the use of an analog low-pass filter before the digital data processing. The required number of terms N generally depends on the bandwidth and the required 'sharpness' of the filter.

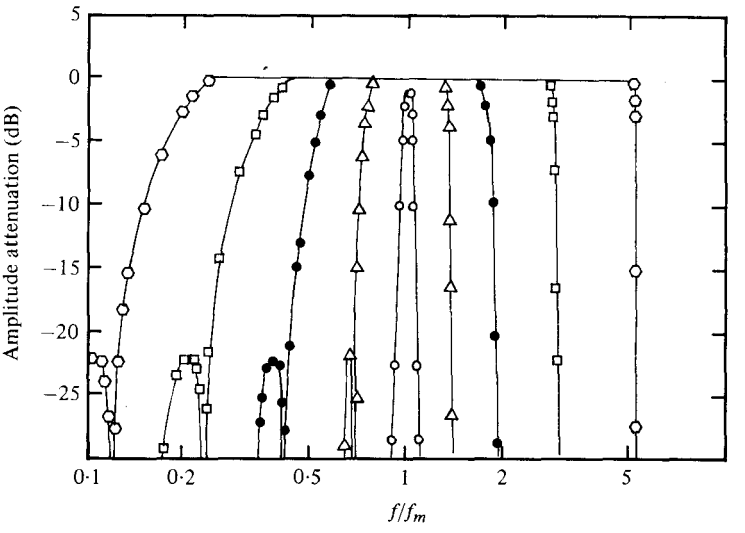

FIGURE 12. Transfer function of a digital, zero phase-shift, band-pass filter. ○, $\Delta f/f_m = 0{\cdot}05$, $N = 50$; △, $\Delta f/f_m = 0{\cdot}6$, $N = 50$; ●, $\Delta f/f_m = 1{\cdot}2$, $N = 25$; □, $\Delta f/f_m = 2{\cdot}5$, $N = 50$; ⬡, $\Delta f/f_m = 5{\cdot}0$, $N = 150$.

Figure 12 shows the amplitude characteristics of the digital filters used in the present study. The sampling time Δt was $1/(2{\cdot}5f_H)$ and the number of terms N for each bandwidth was the lowest one producing reasonably high slopes as well as side lobes with maxima below -20 dB. The first side lobes (corresponding to negative values of the transfer function estimate $\hat{H}(\omega)$) are also shown in figure 12.

REFERENCES

ANTONIA, R. A., CHAMBERS, A. J., VAN ATTA, C. W., FRIEHE, C. A. & HELLAND, K. N. 1978 Skewness of temperature derivative in a heated grid flow. *Phys. Fluids* **21**, 509.

BATCHELOR, G. K. & TOWNSEND, A. A. 1949 The nature of turbulent motion at large wave-numbers. *Proc. Roy. Soc.* A **199**, 238.

BRADSHAW, P. 1967 Conditions for the existence of an inertial subrange in turbulent flow. *Nat. Phys. Lab. Aero. Rep.* 1220.

CHAMPAGNE, F. H. 1978 The fine-scale structure of the turbulent velocity field. *J. Fluid Mech.* **86**, 67.

CORRSIN, S. 1949 An experimental verification of local isotropy. *J. Aero. Sci.* **16**, 757.

CORRSIN, S. 1951 On the spectrum of isotropic temperature fluctuations in an isotropic turbulence. *J. Appl. Phys.* **22**, 469.

CORRSIN, S. 1958 Local isotropy in turbulent shear flow. *N.A.C.A.* RM58B11.

ELENA, M., CHAUVE, M.-P. & DUMAS, R. 1977 Effet de l'aspiration sur les facteurs de dissymétrie et d'aplatissement des dérivées temporelles dans une conduite cylindrique chauffée. *C.R. Acad. Sci. Paris* B **284**, 77.

FRIEHE, C. A., GIBSON, C. H., CHAMPAGNE, F. H. & LA RUE, J. C. 1975 *Atmos. Tech.* **7**, 15.

GIBSON, C. H. & MASIELLO, P. J. 1972 Observations of the variability of dissipation rates of turbulent velocity and temperature fields. In *Statistical Models and Turbulence* (ed M. Rosenblatt and C. Van Atta), Lecture Notes in Physics, vol. 12. Springer.

GIBSON, C. H., FRIEHE, C. A. & MCCONNELL, O. 1977 Structure of sheared turbulent fields. *Phys. Fluids* **20**, S156.

GIBSON, C. H., STEGEN, G. R. & WILLIAMS, R. B. 1970 Statistics of the fine structure of turbulent velocity and temperature fields measured at high Reynolds numbers. *J. Fluid Mech.* **41**, 153.

HARRIS, V. G., GRAHAM, J. A. & CORRSIN, S. 1977 Further experiments in nearly homogeneous turbulent shear flow. *J. Fluid Mech.* **81**, 657.

KENNEDY, D. A. & CORRSIN, S. 1961 Spectral flatness factor and 'intermittency' in turbulence and in non-linear noise. *J. Fluid Mech.* **10**, 366.

KOLMOGOROV, A. N. 1941 The local structure of turbulence in incompressible viscous fluid for very large Reynolds numbers. *C.R. Acad. Sci. U.R.S.S.* **30**, 301.

KUO, A. Y. & CORRSIN, S. 1971 Experiments on internal intermittency and free-structure distribution functions in fully turbulent fluid. *J. Fluid Mech.* **50**, 285.

LAUFER, J. 1951 Investigation of turbulent flow in a two-dimensional channel. *N.A.C.A. Rep.* 1053.

MESTAYER, P. & CHAMBAUD, P. 1979 Some limitations to measurements of turbulence microstructure with hot and cold wires. *Boundary Layer Met.* **16**, 311.

NEVZGLJADOV, V. 1945 A phenomenological theory of turbulence. *C.R. Acad. Sci. U.R.S.S.* **47**, 235.

OBOUKHOV, A. M. 1949 Structure of the temperature field in turbulent flow. *Izv. Akad. Nauk S.S.S.R., Ser. Geogr. i Geofiz.* **13**, 58.

PRANDTL, L. 1925 Bericht über Untersuchungen zur ausgebildeten Turbulenz. *Z. angew. Math. Mech.* **5**, 136.

SANDBORN, V. A. 1959 Measurements of intermittency of turbulent motion in a boundary layer. *J. Fluid Mech.* **6**, 221.

SREENIVASAN, K. R. & ANTONIA, R. A. 1977 Skewness of temperature derivatives in turbulent shear flows. *Phys. Fluids* **20**, 1986.

SREENIVASAN, K. R., ANTONIA, R. A. & DANH, H. Q. 1977 Temperature dissipation fluctuations in a turbulent boundary layer. *Phys. Fluids* **20**, 1238.

SREENIVASAN, K. R. & TAVOULARIS, S. 1980 On the skewness of the temperature derivative in turbulent flows. *J. Fluid Mech.* **101**, 783.

SREENIVASAN, K. R., TAVOULARIS, S., HENRY, R. & CORRSIN, S. 1980 Temperature fluctuations and scales in grid-generated turbulence. *J. Fluid Mech.* **100**, 597.

STEARNS, S. D. 1975 *Digital Signals Analysis.* Rochelle Park, New Jersey: Hayden.

TAVOULARIS, S. 1978 Experiments in turbulent transport and mixing. Ph.D. dissertation, The Johns Hopkins University, Baltimore.

TAVOULARIS, S., BENNETT, J. C. & CORRSIN, S. 1978 Velocity-derivative skewness in small Reynolds number, nearly isotropic turbulence. *J. Fluid Mech.* **88**, 63.

TAVOULARIS, S. & CORRSIN, S. 1981 Experiments in nearly homogeneous turbulence with a uniform mean temperature gradient. Part 1. *J. Fluid Mech.* **104**, 311.

TAYLOR, G. I. 1915 Eddy motion in the atmosphere. *Phil. Trans. Roy. Soc.* A **215**, 1.

UEDA, H. & HINZE, J. O. 1975 Fine-structure turbulence in the wall region of a turbulent boundary layer. *J. Fluid Mech.* **67**, 125.

WYNGAARD, J. C. 1968 Measurement of small-scale turbulence structure with hot-wires. *J. Sci. Instrum.* **1**, 1105.

WYNGAARD, J. C. 1969 Spatial resolution of the vorticity meter and other hot-wire arrays. *J. Sci. Instrum.* **2**, 983.

WYNGAARD, J. C. 1971 Spatial resolution of a resistance wire temperature sensor. *Phys. Fluids* **14**, 2052.